LOSSLESS STORAGE AND TRANSPORTATION LAW OF 250m^3 HORIZONTAL LIQUID HYDROGEN STORAGE TANK

Shouguang Yao*, Xiaoxu Yang

(College of Energy and Power Engineering, Jiangsu University of Science and Technology, Zhenjiang, 212003, Jiangsu, China)

* Corresponding author; E-mail:zjyaosg@126.com

In this paper, the effects of the initial filling rate and heat flux density on the natural convection inside the liquid hydrogen storage tank and the variation laws of temperature and pressure are studied. The study found that the optimal initial filling rate of the 250m^3 liquid hydrogen storage tank was 86%. When the initial filling rate is in the range of 35% to 95%, the change of the heat flux density has a greater impact on the self-pressurization phenomenon than the change of the filling rate. When the initial filling rate is lower than 35%, the pressure in the tank rises sharply, and the change of the initial filling rate has a great influence on the self-pressurization phenomenon. The high initial filling rate and high heat flux density make the pressure rise of the liquid hydrogen storage tank faster during the pressure recovery period. When the liquid hydrogen begins to evaporate in large quantities, the low filling rate and high heat flux make the tank pressure increase faster. By comparing the three thermodynamic models with the simulation results, it is found that the pressure deviation of the 250m^3 liquid hydrogen storage tank with a filling rate of 86% is within 20% calculated by the three-zone model, which is the closest to the simulation results. The deviation of the surface evaporation model at high heat flux density and high filling rate reached 76% and 88.3%, respectively, which was the most affected calculation model by the change of heat flux density and initial filling rate.

Keywords: *Liquid hydrogen storage tanks; Lossless storage and transportation; Thermodynamic models; Pressurization rate; CFD*

1. Introduction

With the wide application of hydrogen energy, cryogenic storage tanks have become the first choice for large-scale long-distance storage and transportation of liquid hydrogen (LH_2) [1,2]. Moreover, the thermal insulation performance of storage tank has high requirements [3]. It is extremely important to study and predict the influencing factors and changing laws of the temperature and pressure changes in the liquid hydrogen storage tank under the application environment conditions.

Experimental testing of the pressurization performance of various storage tanks is the most direct and reliable method. Liebenberg [4] in 1965 used experiments to study the pressurization behavior of a large spherical LH_2 storage tank (208 m^3) under a heat flow of 1.9 W/m^2. The measured pressurization rate is about 10 times higher than that calculated by the system using the saturated homogeneous model. Hasan et al.[5] conducted an experimental study on self-pressurization of small LH_2 storage tanks with a filling rate of 83% and low heat flux density. Experimental data show that the pressurization rate varies nonlinearly with the heat flux density. Dresa et al. [6] and Hastings et al. [7] conducted self-pressurization experiments to obtain the pressurization rates were close to those obtained by Liebenberg [4]. The above experimental

research data covers the influence of various filling rates and heat flux density on self-pressurization.

In view of the superiority of the theoretical calculation of thermodynamic model and the CFD method compared with the experimental method, many researchers have used these two methods to study the self-pressurization effect of storage tanks. Aydelott[8] used the thermodynamic models to study the effect of different filling rates on the self-pressurization of the LH_2 storage tank by numerical calculation. The relevant parameters of the pressurization rate related to the filling rate of the storage tank are obtained. Gursu et al. [9, 10] used three thermodynamic models to analyze the thermal stratification and self-pressurization of small LH_2 cryogenic storage tanks. It was found that the homogeneous model and the surface evaporation model could not accurately predict the experimental data. While the thermal stratification model matched the experimental data well. Lin et al. [11,12] studied the effects of tank size, filling rate and wall heat flow on the pressurization and thermal stratification of spherical LH_2 tanks under microgravity conditions using theoretical calculation methods. However, the model is one-dimensional and does not account for convection in the liquid. Venkat[13] used numerical simulation to explore the influence of filling rate, heat flux density and tank shape on thermo-physical phenomena. However, the mechanism and degree of influence of various influencing factors were not analyzed. Panzarella[14] used numerical simulation to explore the pressurization of large spherical tanks with different filling rates in microgravity. The study found that the final pressurization rate of the tank matched the lumped thermodynamic model of the entire system. Lv[15] et al. used numerical simulation to explore the effect of tank size on the self-pressurization phenomenon in the LH_2 tank. An empirical correlation between the actual pressurization rate and the tank diameter and pressurization rate is proposed. Wang [16] et al. studied the self-pressurization effect of storage tank by using three models: zero dimensional, one-dimensional and CFD. It is found that the three calculation models have accuracy under different conditions. Liu [17,18] explored the self-pressurization effect of cryogenic storage tank under different initial conditions by using the thermal stratification model. Zuo [19] found the best range of evaporation coefficient and condensation coefficient by using the optimization calculation model of self-pressurization process of cryogenic storage tank. The model saves much computational cost. In addition, Seo [20.21] found that the thermal diffusion model and thermal equilibrium model can correctly predict the corresponding pressurization curve under appropriate conditions of liquid nitrogen storage tank. Yao [22] et al. found that the maximum error of pressure change obtained from the modified three zone model and experiment is only about 4.7%. Choi [23] used numerical simulation to compare and analyze the pressure changes of liquid nitrogen and LNG storage tanks under different initial filling rates and different heat flow densities. It can be seen from the above literature that scholars have done research on the variation law and influencing factors of the self-pressurization phenomenon inside the liquid hydrogen storage tank by theoretical calculation, CFD and experimental methods. However, the traditional thermodynamic models are based on some simplified assumptions. It does not have a detailed understanding of the influencing parameters, variation factors and action rules. Therefore, it is necessary to carry out a comparative between the numerical model and different thermodynamic models. This is also the key aspect of lossless storage of cryogenic storage tanks.

In this paper, a $250m^3$ large horizontal liquid hydrogen storage tank is used as the object to establish a numerical analysis model in the process of lossless storage. On the basis of verifying

the reliability of the numerical analysis model, the lossless storage process of the liquid hydrogen storage tank under different filling rates and different heat flux densities was simulated. The influence and mechanism of the initial filling rate and leakage heat flux density on the variation law of the pressurization rate in the tank were analyzed. The calculation results of the pressurization rate are compared with those of the three thermodynamic models. The applicability of each model under different heat flux densities and filling rates is verified by comparing the deviations between the calculation results of the three thermodynamic models and the numerical simulations.

2. Analysis model establishment

2.1 Physical model

This paper takes 250m^3 large horizontal cryogenic storage tank as the research object. The storage tank is composed of a cylindrical inner tank and butterfly heads on both sides. The total length is 26m and the inner tank diameter is 3.7m. The total thickness of the thermal insulation layer is 30mm, the total number of layers is 50, and the thermal conductivity is $2.51*10^{-4}$ W/mK [24,25]. The insulation layer is more complex than LNG storage tanks[26]. The thickness of the inner cylinder is 22.5mm, and the thermal conductivity is 10.7 W/mK. The calculation model takes the middle section of the storage tank. That is, the computational domain is simplified to a circular area with (0,0) as the center and R=1850mm, as shown in Figure 1. An analytical model is established for the two-dimensional gas-liquid two-phase flow and heat and mass transfer.

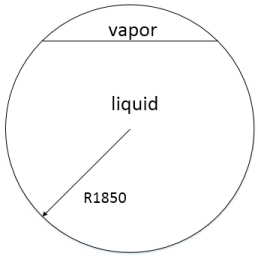

Figure 1 Simplified 2D gas-liquid two-phase diagram for storage tanks

2.2 Mathematical model

The Volume of Fluid (VOF) method was used to predict the motion of the gas-liquid interface. In each cell, the volume fraction is defined as the sum of the volume fractions of the two phases equal to one. Therefore, the volume fractions of the liquid and gas phases can be expressed as:

$$\alpha_l + \alpha_v = 1 \tag{1}$$

In the formula, l is the liquid phase and v is the gas phase. Changes in the gas-liquid interface are studied by solving the governing equations. The liquid hydrogen storage tank satisfies the following equations during lossless storage:

Continuous equation:

$$\frac{\partial \rho}{\partial t} + \nabla\left(\rho \vec{v}\right) = S_m \tag{2}$$

Momentum equation:

$$\frac{\partial}{\partial t}\left(\rho\vec{v}\right)+\nabla\cdot\left(\rho\vec{v}\vec{v}\right)=-\nabla p+\nabla\cdot\left[\mu\left(\nabla\vec{v}+\nabla\vec{v}^{T}\right)\right]+\rho\vec{g}+\vec{F}_{vol} \tag{3}$$

Energy equation:

$$\frac{\partial}{\partial t}\left(\rho E\right)+\nabla\cdot\left(\vec{v}\left(\rho E+p\right)\right)=\nabla\cdot\left(k\nabla T\right)+S_h \tag{4}$$

Field variables and properties are defined in terms of volume fractions.

$$\rho=\alpha_l\rho_l+\alpha_v\rho_v \tag{5}$$

$$\mu=\alpha_l\mu_l+\alpha_v\mu_v \tag{6}$$

$$k=\alpha_l k_l+\alpha_v k_v \tag{7}$$

$$c_p=\frac{1}{\rho}\left(\alpha_l\rho_l c_{pl}+\alpha_v\rho_v c_{pv}\right) \tag{8}$$

The physical properties of hydrogen vary with temperature. The gas phase is set to ideal gas. The energy term E is treated as a mass-averaged variable:

$$E=\frac{\alpha_l\rho_l E_l+\alpha_v\rho_v E_v}{\alpha_l\rho_l+\alpha_v\rho_v} \tag{9}$$

The surface tension at the interface is modeled by a continuum surface force model [27,28]. In this model, surface tension is converted into body force $\vec{F}_{vol}$.

$$\vec{F}_{vol}=\sigma_{lv}\frac{\alpha_l\rho_l\kappa_v\nabla\alpha_v+\alpha_v\rho_v\kappa_l\nabla\alpha_l}{0.5\left(\rho_l+\rho_v\right)} \tag{10}$$

In the formula, σ_{lv} represents the interfacial surface tension, κ_v and κ_l are the surface curvatures calculated from the local gradient of the surface normal at the interface. They can be expressed as:

$$\kappa_l=\frac{\nabla\alpha_l}{\left|\nabla\alpha_l\right|}\quad\kappa_v=\frac{\nabla\alpha_v}{\left|\nabla\alpha_v\right|} \tag{11}$$

The Herz-Knudsen equation describing the evaporation problem:

$$J'=\alpha_c\frac{\sqrt{M}}{\sqrt{6.28R}}\left(\frac{P}{\sqrt{T_v}}-\frac{P_{sat}T_l}{\sqrt{T_l}}\right) \tag{12}$$

Clausius Clapeyron's equation for vapor pressure describing the gas-liquid equilibrium:

$$\frac{dP}{dT}=\frac{\Delta H}{T\left(\frac{1}{\rho_v}-\frac{1}{\rho_l}\right)} \tag{13}$$

After deduction, the mass flow at the gas-liquid interface during the evaporation and condensation process is obtained as:

$$J_{lv}=r_l\alpha_l\rho_l\left(T-T_{sat}\right)/T_{sat}\qquad J_{v\,l}=r\alpha\,\rho\,\left(_vT-\;\;T\right)/_{a\;t}\;T \tag{14}$$

T_{sat} is the saturation temperature, which varies with the pressure inside the tank according to the Clausius-Clapeyron equation. The Lee model was used to consider the mass transfer process [29], and $r_{eva}=0.00001$, $r_{con}=0.0001$ were obtained by trial and error [30]. Mass and heat exchange is always exist in the gas-liquid two phases of the liquid hydrogen storage tank. This article deals with the exchange of mass and heat as follows:

$$\mathrm{Sm}=\begin{cases} r_{eva}\alpha_l\rho_l\left(T_l-T_{sat}\right)/T_{sat} & T_l\geq T_{sat} \\ r_{con}\alpha_v\rho_v\left(T_v-T_{sat}\right)/T_{sat} & T_v<T_{sat} \end{cases} \tag{15}$$

$$S_h=S_m\Delta H \tag{16}$$

In the formula, S_m is the quality source item, S_h is the energy source term, T_{sat} is the evaporation temperature, $\alpha_c=1$ is the evaporative condensation regulation coefficient, J' is the net mass flux between the gas and liquid phases, $kg/(m^2\cdot s)$; α is the phase fraction, ρ is the density, kg/m^3, l and v represent the liquid and gas phases, respectively; ΔH represents the latent heat of evaporation, $kJ/kmol$. UDF (User defined function) programming was used to import the source term equation of heat and mass exchange between gas and liquid into FLUENT software to simulate the heat and mass transfer between gas and liquid during lossless storage.

2.3 Boundary and initial conditions

It is assumed that the tank wall is heated by a constant heat flux. According to the size of the liquid hydrogen storage tank, the environmental conditions, the qualitative temperature of the fluid in the storage tank, etc., the formula of the leakage heat flux density on the inner wall of the storage tank is deduced as:

$$q=\frac{\pi L\left(t_{fi}-t_{f0}\right)}{\dfrac{1}{h_lD}+\ln\left(D+2\delta_1/D\right)/2\lambda_1+\ln\left(D+2\delta_1+2\delta_2/D+2\delta_1\right)/2\lambda_2+\dfrac{1}{h_gD+2\delta_1+2\delta_2}}{\pi DL} \tag{17}$$

In the formula, q is the heat flux density, w/m^2; L is the length of the middle cylindrical part of the tank, mm; D is the inner diameter of the tank, mm; δ_1 is the inner tank wall thickness, mm; δ_2 is the thickness of the insulation layer, mm; t_{fi} is the fluid average temperature, K; t_{f0} is the ambient temperature, 293K, h_l and h_g are the convective heat transfer coefficients of the internal storage liquid and the external air, respectively. $w/(m^2K)$; The initial pressure is 101325Pa. The initial temperature is the corresponding saturation temperature at the initial pressure, 20.37K. It is assumed that the initial temperature is the same throughout the liquid and gas phases. Moreover,

set the inner wall surface as a no-slip boundary. Substituting the environmental parameters under an atmospheric pressure into Formula 1, the heat flux density of liquid hydrogen storage tank with initial filling rate of 95% is 2.2559 W/m^2. In order to explore the influence of the change of initial filling rate and heat flux density on the pressure of storage tank, the heat flux density is gradually increased by 15% and the initial filling rate is reduced by 15%. In this paper, 12 working conditions are simulated. The initial conditions and tank parameters corresponding to each working condition are shown in Table 1.

Table 1 Initial and boundary conditions for each case

Number	Filling rate(%)	Heat flux (W/m^2)	Number	Filling rate (%)	Heat flux (W/m^2)
1	95%	2.2559	7	20%	2.2559
2	86%	2.2559	8	86%	2.5943
3	80%	2.2559	9	86%	2.9834
4	65%	2.2559	10	86%	3.4309
5	50%	2.2559	11	86%	3.9456
6	35%	2.2559	12	86%	4.5374

2.4 Turbulence model

According to the initial pressure of the liquid hydrogen storage tank at the initial time of 1 atm, the temperature of the storage tank at this time is 20.37K, and the heat flux density is 2.2559W/m^2. The Gr number is obtained as $Gr = 2.9829 \times 10^{15}$. The natural convection inside the tank is turbulent. The Realizable $k-\varepsilon$ turbulence model is selected for this simulation [31,32]. In the Realizable $k-\varepsilon$ turbulence model, the distance between the fluid near the wall and the wall mesh should be small enough to ensure that the near-wall region is always a viscous bottom layer. The y+ value closest to the solid wall is within the allowable range of the computational turbulence model. Based on the literature [33], y+ is set to 4~5.

2.5 Solution settings

According to the established physical model, the computational domain is divided into unstructured meshes by ICEM software. The grid near the wall and gas-liquid interface is refined, as shown in Figure 3. The VOF method is used to deal with the gas-liquid two-phase problem. Unsteady calculations are performed using a pressure-based solver. For the thermodynamic physical properties and migration properties of hydrogen, the calculation formulas of various related parameters were fitted by polynomials and imported into the material library. The mass source term and energy source term in the control equation are imported into the FLUENT software using UDF. The pressure-velocity coupling calculation was carried out using the PISO method. For the pressure interpolation required to solve the momentum equation, a body force weighted method is used. The discrete formats for momentum and energy use a second-order upwind format. The mass and momentum residual values are set to 10^{-3}, while the energy residual values are set to 10^{-6}.

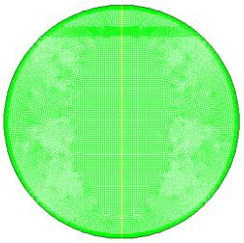

Figure 2. 2D Computational Grid

3. Calculation process

3.1 Grid independence analysis

In order to ensure the accuracy of the simulation, this paper conducts grid independence research on the gas pressure inside the liquid hydrogen storage tank with a filling rate of 95% and a heat flux density of 2.2559 W/m^2 within 13 hours. The grid numbers are 9168, 14385, 25350, respectively. The initial pressures are all 101325Pa. Table 2 shows the gas pressure distribution of the three grid-number models when the liquid hydrogen storage tank is given a step size of 0.02 within 13 hours. It can be seen from Table 2 that the pressure changes of the three grids are basically the same. However, the error of the coarse grid is relatively large, so the model with the grid number of 14385 can meet the grid-independent requirements.

Table 2. Three kinds of grid numbers to calculate the gas pressure value and deviation at a given step size of 0.02 for 13h

Grid number	9168	14385	25350
Gas pressure (Pa)	111200.6	106827.76	105209.94
Calculation error	4.09%	1.5%	

3.2 Model Validation

In order to verify the correctness of this model, liquid nitrogen is first selected for simulation. This data is compared with the experimental data of lossless storage of liquid nitrogen storage tanks in literature [22]. Because it is very dangerous to carry out liquid hydrogen experiment directly, safe liquid nitrogen is selected to verify the feasibility of the model. Figure 3 shows the comparison between the simulation results and the experimental results. It can be seen from the figure that the deviation between the simulation results and the experimental results is generally not more than 7%. The pressure obtained from the simulation in the initial stage is in good agreement with the experimental results. The later simulation results have a large deviation from the experimental results. And the time when the pressure obtained from the experiment enters the fast-growing region is earlier than the simulation result. The reason should be that in order to simplify the calculation, the established analytical model ignores the heat leakage of the heads at both ends of the tank. Therefore, the total heat leakage in the simulation is slightly lower than the actual situation. As a result, the formation of the thermal stratification region under the gas-liquid interface in the simulation is slower than the actual one. The time point of the rapid rise of the gas-phase space pressure is relatively late. The verification shows that the hypothesis and the numerical analysis model established in this paper are reliable.

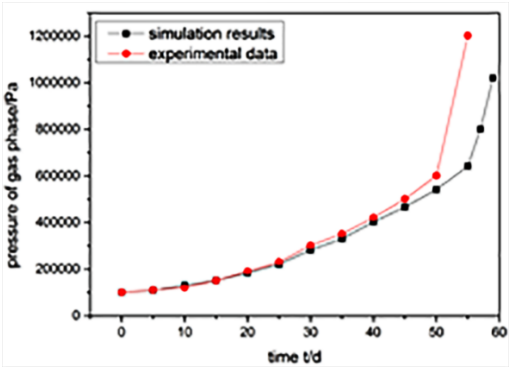

Figure 3. Comparison of liquid nitrogen simulation and experimental data

4. Results Analysis

4.1 Internal pressure analysis

Figure 4 shows the variation law of gas phase pressure in the LH_2 storage tank with time under different heat flux densities and different filling rates. It can be seen from the figure that the internal pressure of the storage tank gradually increases with the increase of time. The pressurization rate in the storage tank corresponding to each stage is different under the conditions of different filling rates and different heat flux densities. The pressure change consists of three stages. The first stage gas phase space pressure is reduced. This is because the gas phase begins to condense. The pressure drop of the tank is small at low filling rate and high heat flux density. The gas phase absorbs more heat when the tank is at a low fill rate and high heat flux density. The condensation rate is reduced and the pressure drop is smaller. The second stage is the liquid phase begins to thermally expand and compress the gas phase, resulting in a gradual increase in pressure inside the tank. The condensation stage ends. At this time, the pressure increase rate under the condition of high filling rate is greater than that of low filling rate. The third stage is that with the increase of time, the temperature of the liquid phase at the gas-liquid interface reaches the saturation temperature. After the temperature continues to rise, a phase change occurs in the storage tank. Part of the liquid phase evaporates, resulting in a rapid increase in the gas phase pressure in the tank.

It can be seen from Fig. 4(a) that as the filling rate decreases, the pressure rise rate first decreases and then increases. It can be seen from Fig. 4(b) that the pressure rise rate in the tank increases continuously with the increase of heat flux density. The comparison between the two figures shows that the uniform change of initial filling rate can’t make the uniform change of pressure rise rate.

Table 4 shows the rate of increase in tank pressure under different conditions. It can be seen from the table that within the range of the initial filling rate from 35% to 80%, for every 15% increase in the initial filling rate, the pressure increase rate increases by an average of 53.86%. In the range of heat flux density 2.5943W/m^2~3.9456 W/m^2, for every 15% increase in heat flux density, the pressure increase rate increases by 54.05% on average. When the initial filling rate was within 20%~35%, the pressure increase rate increased sharply, increasing by 70.01%. It is higher than 68.01% of the heat flux density. It can be seen that in a certain range of high initial filling rate, the pressure increase rate is more seriously affected by the change of heat flux density. When the filling rate is extremely low, the change in the filling rate has a greater impact on the pressure in the tank. In addition, when the initial filling rate is in the range of 80% to 95%, the

pressure increase rate does not change much. Especially when the initial filling rate is 86%, the pressurization rate in the tank is the smallest. Therefore, within the range of 80% to 95% of the initial filling rate, 86% is the best initial filling rate.

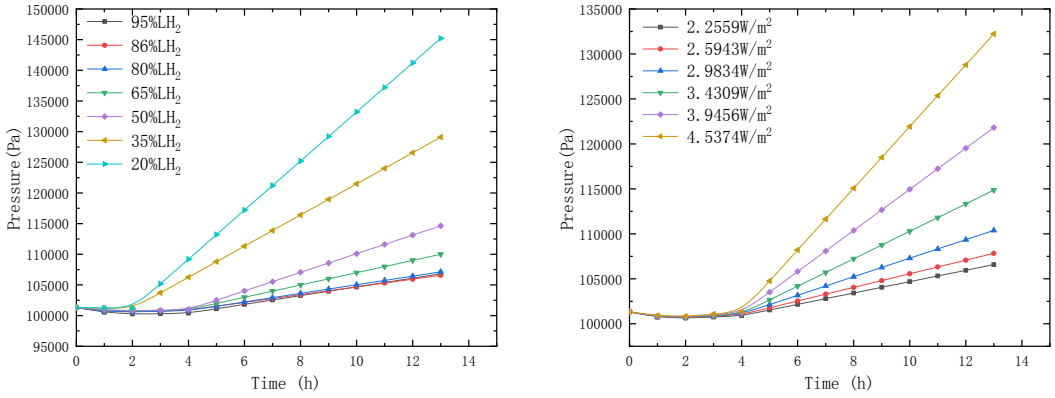

a b

Figure 4. Tank pressure diagrams under different filling rates (a) and different heat flux densities (b)

Table 3 The rate of pressure rise in the tank under different working conditions

Number	Filling rate（%）	Heat flux（W/m^2）	$\left.\frac{dp}{dt}\right\|_n$（Pa/h）
1	95	2.2559	713.44
2	86	2.2559	630.9
3	80	2.2559	700.9
4	65	2.2559	1002.75
5	50	2.2559	1516.2
6	35	2.2559	2537.2
7	20	2.2559	4313.24
8	86	2.5943	757.13
9	86	2.9834	1092.16
10	86	3.4309	1674.83
11	86	3.9456	2756.1
12	86	4.5374	4130.52

4.2 Influence mechanism of self-pressurization rate of liquid hydrogen storage tank

Early storage stages assume that the gas phase region is at a uniform temperature. Combining the mass and energy conservation equations, the state equation and the heat definition, the gas-phase pressurization rate is obtained as [34]:

$$\frac{dp}{dt}=\frac{\left(\beta_v Q_v / c_{p,v}\right)+m_e-\rho_v\left(dV_v / dt\right)}{\rho_v V_v \kappa_v\left(c_{v,v} / c_{p,v}\right)} \tag{19}$$

In the formula, β_v is the thermal expansion coefficient of the gas phase; ρ_v is the vapor

density; Q_v is the heat input rate of the gas phase; $c_{p,v}$ is the constant pressure specific heat of the gas phase; $c_{v,v}$ is the constant volume specific heat of the gas phase; m_e is the net mass transfer rate at the liquid-gas interface; V_v is the gas volume; κ_v is the isothermal compressibility of the gas phase. Assume that the early storage stages β_v、ρ_v、$c_{p,v}$、$c_{v,v}$、κ_v and c are fixed values.

It can be seen from equation (19) that the pressure rise rate is affected by 3 parts. The first term is the pressure increase caused by the direct heat absorption of the gas phase. The second term is the pressure increase caused by the phase transition. The third term is the pressure change due to thermal expansion of the heated liquid phase and subsequent compression of the gas phase region. When the heating rate of the gas phase is constant, the higher the filling rate, the smaller the volume of the gas phase. The pressure rise caused by the direct sensible heat input in the gas phase is faster. During condensation, m_e is negative. When the filling rate is high, the temperature gradient of the gas-liquid interface is small. The absolute value of $\frac{m_e}{V_v}$ also decreases accordingly. The pressure caused by the phase transition is also increasing rapidly. For $-\frac{1}{V_v}\frac{dV_v}{dt}$, the relationship between gas pressure and volume is derived from the equation of state:

$$\frac{\Delta p}{p} \propto \frac{-\Delta V_v}{V_v} \tag{20}$$

The gas phase volume change value $-\Delta V_v$ caused by the thermal expansion of the liquid is roughly the same at high and low filling rate levels. For a given storage tank, the larger the filling rate, the more significant the effect of liquid thermal expansion on the pressure rise of the storage tank.

With the continuous increase of the heat leakage of the storage tank, the convection intensity in the gas phase region increases. The evaporation of the liquid phase is accelerated. The temperature inside the tank is no longer evenly distributed, resulting in increased thermal stratification. Equation (19) is no longer suitable for analyzing the rate of pressure change. Combining the mass and energy conservation equations, the state equation and the definition of heat, the gas phase pressurization rate at this stage is obtained as [6]:

$$\frac{dp}{dt} = \frac{1}{\rho_l}\left(\frac{\partial p}{\partial u}\right)_\rho \frac{Q_w}{V_l} \tag{21}$$

In the formula, u is the specific internal energy; Q_w is the wall heat flux density; V_l is the liquid volume; ρ_l is the liquid density. It can be seen from the formula that when the heat flux

density is constant, the lower the filling rate, the faster the pressure rise rate. It can be seen from formula (19) that when the filling rate is constant, the increase of heat flux accelerates the heat input rate of gas phase. The pressure rise caused by gas phase direct sensible heat input is faster. During condensation, the increase of heat flux leads to the decrease of temperature gradient at the gas-liquid interface. The absolute value of $\frac{m_e}{V_v}$ also decreases. The pressure caused by phase transition is also increasing. For a given tank, the increase of heat flux makes the effect of liquid thermal expansion on the pressure rise of the tank more significant. When a large amount of liquid phase begins to evaporate, the pressure change trend in the tank is judged according to formula (21). It can be seen from formula (21) that when the filling rate is a fixed value, the greater the heat flux is, the faster the pressure rises.

4.3 Comparative analysis of pressurization rate under different filling rates

Figure 5 shows the comparison between the pressure values of the numerical simulation in the tank and the values calculated by the three traditional thermodynamic models. This comparison was made at initial fill rates of 86% and 50% and heat flux density of 2.2559W/m^2. It can be seen from the figure that the pressure at the initial time is 101325Pa, which is simulated for 13 hours. With the increase of storage time, the pressure calculated by each model first decreased and then increased, but the pressurization rate was different. As can be seen from figure 5 (a), the surface evaporation model is 1912Pa higher than the numerical simulation calculation result. The calculated result of saturated homogeneous model is 1801Pa lower than that of numerical model. At this time, the deviation between the pressure curve calculated by the surface evaporation model and the simulation result curve is the largest. As can be seen from figure 5 (b), the calculation result of surface evaporation model is 2802.76Pa higher than the numerical calculation result. The calculated result of saturated homogeneous model is 3291.98Pa lower than that of numerical model. The deviation between the calculation results of saturated homogeneous model and simulation is the largest. The deviation of the surface evaporation model calculation result curve and the simulation result curve decreases with the decrease of the filling rate. This is due to the fact that the higher the proportion of liquid phase, the more energy is absorbed, and more evaporation occurs, resulting in a higher pressurization rate. In contrast, the saturated homogeneous model produces computational bias for the opposite reason. Higher fill rates require more heat to maintain a constant tank temperature. Therefore, despite the increase in heat, the pressurization rate decreases. The calculation result of the improved three-zone model at different filling rates is the closest to the simulation results. The reduction in the fill rate also increases the deviation from the simulation results.

Table 5 shows the pressurization rates calculated by different thermodynamic models and numerical simulations. It can be seen from the table that when the filling rate is 86%, the deviation of the surface evaporation model from the simulated value reaches 76%. The deviation is 9.9% when the initial filling rate is 50%. The deviations of the saturated homogeneous model and the three-zone model from the simulation calculations are 32.8% and 10.2% when the initial filling rate is 86%. The calculated deviations when the initial filling rate is 50% are 25.6% and 8.9%. The lower initial fill rate results in smaller deviations from the simulation calculations. It can be seen from the table that when the initial filling rate is high, the saturated homogeneous model has less

error than the surface evaporation model. The error of the surface evaporation model is small when the initial filling rate is low. The two calculation models are greatly affected by the change of the initial filling rate. The calculation results of the three-zone model under different initial filling rates are in good agreement with the simulation results. The deviation from the simulation results did not increase significantly with time.

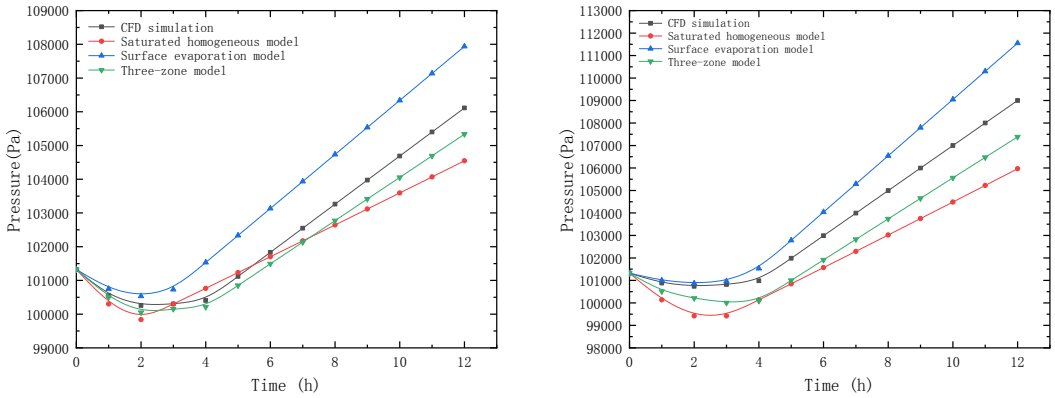

Figure 5. Variation of tank pressure with time at initial filling rate of 86% (a) and 50% (b) with different calculation methods

Table 5. Pressurization rate at different initial filling rates

Working fluid	Filling rate (%)	Heat flux (W/m^2)	$\left.\frac{dp}{dt}\right\|_n$ (Pa/h)	$\left.\frac{dp}{dt}\right\|_h$ (Pa/h)	$\left.\frac{dp}{dt}\right\|_s$ (Pa/h)	$\left.\frac{dp}{dt}\right\|_t$ (Pa/h)
LH_2	86%	2.2559	630.9	424.22	1107.73	566.42
LH_2	50%	2.2559	1516.2	1128.51	1666.15	1379.74

4.4 Comparative analysis of pressurization rates under different heat flux densities

The simulation results of different heat flux densities are compared with the calculation results of the thermodynamic models to explore the variation law and calculation deviation of the calculation results of the thermodynamic models under different heat flux densities. Figure 6 shows the comparison of the tank pressure calculated by the three traditional thermodynamic models with the numerical simulation results. These comparisons were made with an initial fill rate of 86% and heat fluxes of 2.2559W/m^2 and 3.9456W/m^2. As can be seen from Figure 6 (b), the surface evaporation model is 26330.43Pa higher than the numerical simulation calculation result. The calculated result of saturated homogeneous model is 3787Pa lower than that of numerical model. It can be seen from the figure that as the heat flux density increases, the deviation of the surface evaporation model from the numerical simulation gradually increases. The deviation of the saturated mean model from the simulation calculation gradually narrowed. The calculation results of the three-zone model under different heat flux densities are the closest to the simulation results. The deviation from the simulation results did not increase significantly with the increase of the lossless storage time.

Table 6 shows the pressurization rates for different thermodynamic models and simulation results. When the heat flux density is 3.9456W/m^2, the pressure rise rate calculated by the surface evaporation model deviates by 88.3% from the simulation results, which is higher than 75.58%

when the heat flux density is 2.2559W/m^2. This is due to the high heat flux that accelerates the evaporation of the storage tank, causing a rapid increase in pressure. The deviation of the saturated homogeneous model is much lower at high heat flux than the calculated deviation at low heat flux, with a value of 0.62%. This is because the high heat flux makes the temperature inside the tank rise rapidly, and the pressure rises with it. It can be seen that the change of heat flux density has a greater impact on the deviation of the pressure of the liquid hydrogen storage tank calculated by the surface evaporation model. The deviation between the three zone model and the numerical simulation results is very small at both heat flux densities.

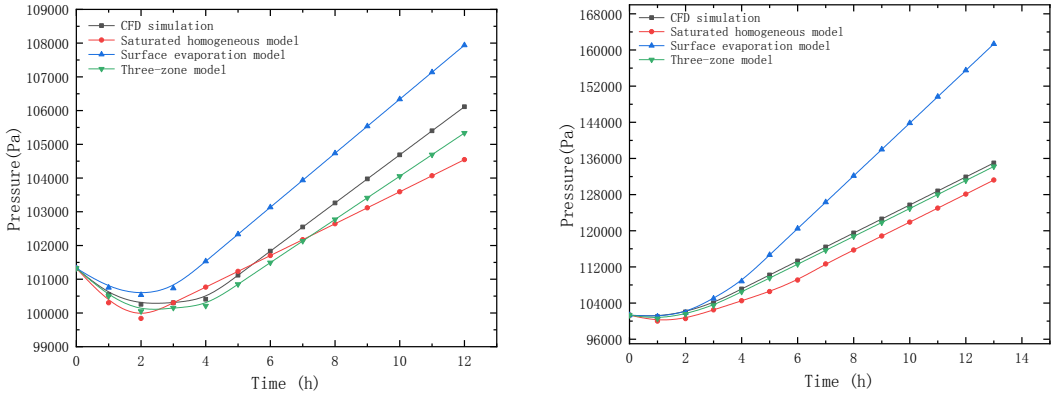

Figure 6. The relationship between the pressure and time of the liquid hydrogen storage tank with the initial filling rate of 86% and the heat flux density of 2.2559W/m^2(a) and 3.9456W/m^2(b)

Table 6. Pressurization rates at different heat flux densities

Working fluid	Filling rate (%)	Heat flux (W/m^2)	$\left.\frac{dp}{dt}\right\|_n$ (Pa/h)	$\left.\frac{dp}{dt}\right\|_h$ (Pa/h)	$\left.\frac{dp}{dt}\right\|_s$ (Pa/h)	$\left.\frac{dp}{dt}\right\|_t$ (Pa/h)
LH_2	86%	2.2559	630.9	424.22	1107.73	566.42
LH_2	86%	3.9456	2756.1	2773.19	5188.637	2756.19

4.5 Mechanism analysis of calculation deviation of three thermodynamic models

Since the pressure of liquid hydrogen storage tank is calculated according to the saturation temperature at the gas-liquid interface, it is necessary to compare and analyze the temperature at the gas-liquid interface. Figure 7 and figure 8 show the temperature change law at the gas-liquid interface calculated by numerical simulation and three thermodynamic models under different initial filling rates and different heat flux densities. With the increase of lossless storage time, the temperature at the gas-liquid interface keeps rising. Different models have different temperature rise rates. As can be seen from figure 7, the temperature deviation of the saturated homogeneous model gradually increases with the decrease of the initial filling rate. The calculation deviation of surface evaporation model is relatively small. The temperature calculated by the three zone model always has little deviation from the CFD simulation. As can be seen from figure 8, with the increase of heat flux, the temperature deviation calculated by saturated homogeneous model and surface evaporation model increases. The calculation deviation of the three zone model changes

little. The temperature change law presented here matches the pressure change law in the figure above. This shows that the temperature at the gas-liquid interface determines the deviation of pressure calculation results. The accuracy of the assumptions of the three thermodynamic models is the key to the calculation of tank pressure by the thermodynamic model.

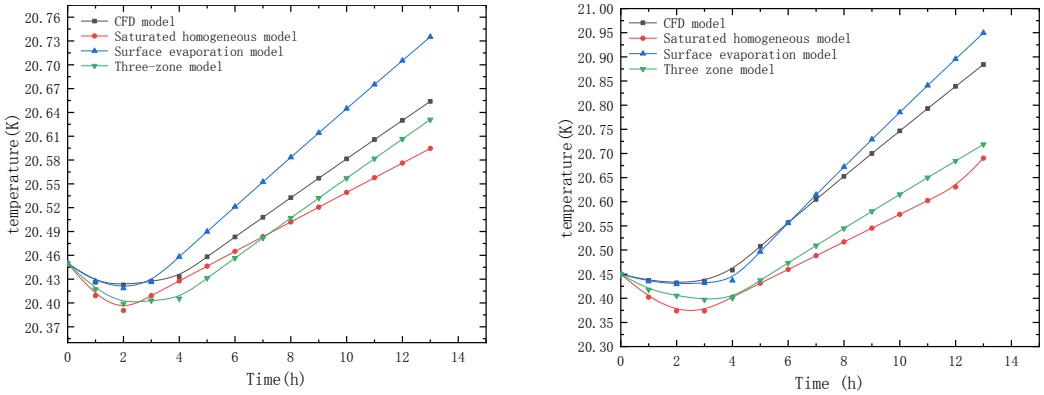

Fig.7 Temperature variation at gas-liquid interface at initial fill rate of 86% and 50%

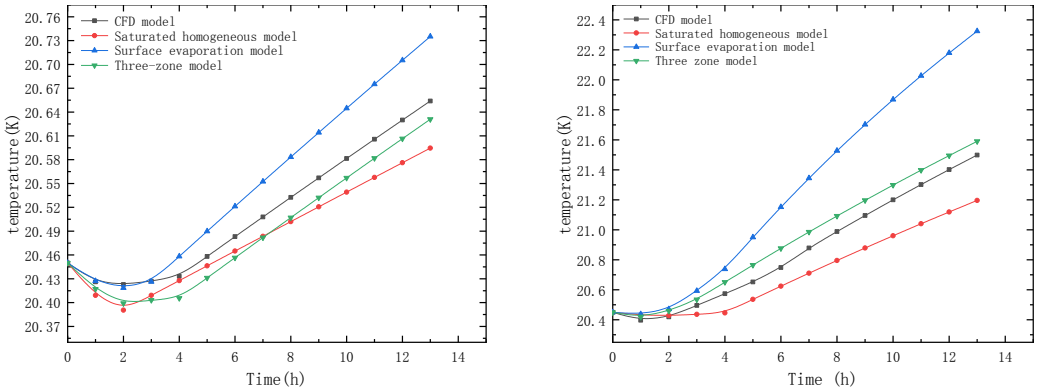

Fig.8 Temperature variation at gas-liquid interface at heat flux 2.2559 W/ m^2 and 3.9456 W/ m^2

5 Conclusion

The pressure of the 250m^3 liquid hydrogen storage tank under different filling rates and different heat flux densities first decreased, then slowly increased and finally increased linearly. When the initial filling rate varies from 50% to 95%, the change of heat flux density has a greater influence on the pressurization rate in the tank. When the initial filling rate varies from 20% to 35%, its influence on the pressurization rate in the tank is higher than that of the heat flux density.

The initial filling rate of 86% is the best initial filling rate of the 250m^3 liquid hydrogen storage tank. In addition, when the initial filling rate of the volume storage tank is less than 35%, the pressure in the tank rises sharply and quickly reaches the safe pressure value of the storage tank, which endangers the safe use of the liquid hydrogen storage tank.

The saturated homogeneous model and the surface evaporation model are greatly affected by changes in filling rate and heat flux density, especially by heat flux density. The 250m^3 liquid hydrogen storage tank uses the saturated homogeneous model and the surface evaporation model to predict that the deviation of the pressure growth rate decreases with the decrease of the filling rate. Among them, the surface evaporation model has a larger reduction, but it is still more than 25%. When the heat flux density increases, the calculation deviation of the surface evaporation model increases, and the error exceeds 50%. However, the calculation deviation of the saturated

homogeneous model is reduced, and the error does not exceed 5%. The deviation of the three-zone model under different initial filling rates and different heat flux densities from the simulated values is the smallest.

Nomenclature

F_{vol} Body force [N/m^3]	κ Surface curvature [1/m]
E Energy term [J]	ρ Density [kg/m^3]
J' Mass flow rate [kg/(m^{2}s)]	α Volume of fluid fraction
S Source item [W/m^3]	μ Dynamic viscosity [m^2/s]
ΔH Latent heat [KJ/kmol]	δ Wall thickness [m]
L Middle cylinder length [m]	Subscripts
D Tank diameter [m]	l Liquid
T Temperature [K]	v Vapor
C_p Specific heat at constant pressure [J/(kgK)]	sat Saturation
q Heat flux [W/m^2]	n numerical simulation
h Convective heat transfer coefficient [W/(m^{2}K)]	h homogeneous model
λ Thermal conductivity [W/(mK)]	s Surface evaporation model
σ Surface tension [N/m]	t Three zone model

References

[1] Ratnakar R R, *et al*. Hydrogen supply chain and challenges in large-scale LH_2 storage and transportation, *International Journal of Hydrogen Energy*, 46(2021),47,pp. 24149-24168

[2] Wang S. Beyond design basis seismic evaluation of underground liquid storage tanks in existing nuclear power plants using simple method, *Nuclear Engineering and Technology*, (2021)

[3] D. Salomone, *et al*. Modeling of heat leak effect in round trip efficiency for Brayton pumped heat energy storage with liquid media, by cooling and heating of the reservoirs tanks, *Journal of Energy Storage*, 46(2022), pp.103793

[4] D.H. Liebenberg, *et al*. Pressurization analysis of a large-scale liquid hydrogen dewar, *Plenum Press*, (1965), pp. 284-289

[5] M.M. Hasan, *et al*. Self-pressurization of a flight-weight liquid. hydrogen storage tank subjected to low heat flux, *Am. Soc. Mech. Eng. Heat Transf. Div. HTD*. 167(1991),pp. 37-42

[6] N.T. Van Dresar, *et al*. Self-pressurization of a flightweight liquid hydrogen tank - Effects of fill level at low wall heat flux, *AIAA*, 1992, 2, pp. 92-95

[7] LJ. Hastings, *et al*. Spray bar zero-gravity vent system for on-orbit liquid hydrogen storage,

NASA/TM-2003-212926, 2003

[8] J.C. Aydelott, *et al*. Effect of size on normal-gravity self- pressurization of spherical liquid hydrogen tankage, *NASA/TM-D-5196*, 1969

[9] Gursu S, et al. Analysis and Optimization of Thermal Stratification and Self-Pressurization Effects in Liquid Hydrogen Storage Systems—Part 1: Model Development, *Journal of Energy Resources Technology*, 115 (1993),3, pp. 221-227

[10] Gursu S , et al. Analysis and Optimization of Thermal Stratification and Self-Pressurization Effects in Liquid Hydrogen Storage Systems—Part 2: Model Results and Conclusions, *Journal of Energy Resources Technology*, 115(1993),3, pp. 228-231

[11] Lin C S , *et al*. Self-pressurization of a spherical liquid hydrogen storage tank in a microgravity environment, *estuarine coastal & shelf science*, 1992

[12] Lin C S, *et al*. Pressure Control Analysis of Cryogenic Storage Systems, *Journal of Propulsion and Power*, 20(2004), 3, pp. 480-485

[13] Venkat S, *et al*. Self-Pressurization and Thermal Stratification in a Liquid Hydrogen Tank Under Varying Gravity Conditions, *42nd AIAA Aerospace Sciences Meeting and Exhibit*, 2004

[14] Panzarella C H, *et al*. Self-Pressurization of Large Spherical Cryogenic Tanks in Space, *Journal of Spacecraft and Rockets*, 42(2005), 2, pp. 299-308

[15] Lv R, *et al*. Thermodynamic Analysis of a Partially Filled Hydrogen Tank in a wide scale range, *Applied Thermal Engineering*, 193(2021), 6, pp. 117007

[16] Lei W, *et al*. Comparison of three computational models for predicting pressurization characteristics of cryogenic tank during discharge, *Cryogenics*, 65(2015), pp. 16-25

[17] Liu Z, *et al.* Development of thermal stratification in a rotating cryogenic liquid hydrogen tank, *International Journal of Hydrogen Energy*, 40(2015), 43, pp. 15067-15077

[18] Liu Z, *et al*. Effect of initial parameter on thermodynamic performance in a liquid oxygen tank with pressurized helium gas, *Science and Technology for the Built Environment*, (2019), pp. 1-32

[19] Zuo Z, *et al.* A numerical model for liquid-vapor transition in self-pressurized cryogenic containers, *Applied Thermal Engineering*, 193(2021), pp. 117005

[20] Seo M , *et al*. Thermodynamic analysis of self-pressurized liquid nitrogen cryogenic storage tank, *Jsme-ksme Thermal & Fluids Engineering Conference.* 2008

[21] Mansu Seo, *et al*. Analysis of self-pressurization phenomenon of cryogenic fluid storage tank with thermal diffusion model, *Cryogenics*, 50(2010), 9, pp. 549-555

[22] S, Yao, *et al.* Experimental and Theory Study of the Lossless Storage Law for Marine LNG Storage Tank Based on Modified Three-District Model, *The Open Petroleum Engineering Journal*, 7(2014), 1, pp. 104-108

[23] Choi S W, *et al*. Numerical analysis of convective flow and thermal stratification in a cryogenic storage tank, *Numerical Heat Transfer Part A Applications*, 71(2017), 4, pp. 402-422

[24] Kumar S S, *et al.* Design and Analysis of Hydrogen Storage Tank with Different Materials by Ansys, *IOP Conference Series Materials Science and Engineering*, 810(2020), pp. 012016

[25] Tsipianitis A ,*et al*. Optimizing the seismic response of base-isolated liquid storage tanks using swarm intelligence algorithms, *Computers & Structures*, 243(2021), 15, pp. 106407

[26] Lisowski E., *et al.* Study on thermal insulation of liquefied natural gas cryogenic road tanker,

Thermal Science, 23(2019), pp. S1381-S1391
[27] J. Brackbill, *et al*. A continuum method for modeling surface tension, *J. Comput. Phys*. 100 (1992), pp. 335-354
[28] Fu J, et al. Influence of phase change on self-pressurization in cryogenic tanks under microgravity, *Applied Thermal Engineering*, 87(2015), pp. 225-233
[29] H. Lee, A Pressure Iteration scheme for two-phase flow modeling, T.N. Veziroglu (Ed.), Multiphase Transport Fundamentals, Reactor Safety, Applications, 1, Hemisphere Publishing, Washington, DC, (1980)
[30] Z.Y. Liu, *et al*. VOF modelling and analysis of filmwise condensation between vertical parallel plates, *Heat Transfer Research* 43(2012), pp. 47–68
[31] L. Wang, *et al*. CFD investigation of thermal and pressurization performance in LH_2 tank during discharge, *Cryogenics*, 57(2013), pp. 63-73
[32] L. Wang, *et al*. Transient thermal and pressurization performance of LO_2 tank during helium pressurization combined with outside aerodynamic heating, *Int. J. Heat Mass Transf.* 62(2013), pp. 263-271
[33] B.F. Inc, Fluent User's Guide, in: Fluent Incorporated, Lebanon NH, 2010
[34] J.S. Brown, Vapor condensation on turbulent liquid, Massachusetts Institute of Technology, 1991.

Submitted: 28.2.2022.
Revised: 20.5.2022.
Accepted: 24.5.2022.